Electron-impact dissociative excitation and ionization of N_2D^+

M. Fogle*
Department of Physics, Auburn University, Auburn, Alabama 36849, USA

E. M. Bahati, M. E. Bannister, S. H. M. Deng, and C. R. Vane
Physics Division, Oak Ridge National Laboratory, Oak Ridge, Tennessee 37831, USA

R. D. Thomas and V. Zhaunerchyk
Department of Physics, Albanova, Stockholm University, SE-106 91 Stockholm, Sweden

(Received 1 August 2011; published 22 September 2011)

Absolute cross sections for electron-impact dissociation of N_2D^+ producing N_2^+, ND^+, and N^+ ion fragments were measured in the 5- to 100-eV range using a crossed electron-ion beams technique. In the 5- to 20-eV region, in which dissociative excitation (DE) is the principal contributing mechanism, N_2^+ production dominates. The $N_2^+ + D$ dissociation channel shows a large resonant-like structure in the DE cross section, as observed previously in electron impact dissociation of triatomic dihydride species [M. Fogle, E. M. Bahati, M. E. Bannister, S. H. M. Deng, C. R. Vane, R. D. Thomas, and V. Zhaunerchyk, Phys. Rev. A **82**, 042720 (2010)]. In the dissociative ionization (DI) region, 20- to 100-eV, N_2^+, ND^+, and N^+ ion fragment production are comparable. The observance of the ND^+ and N^+ ion fragments indicate breaking of the N−N bond along certain dissociation channels.

DOI: 10.1103/PhysRevA.84.032714 PACS number(s): 34.80.Gs, 34.80.Ht

I. INTRODUCTION

Collisions of free electrons with atomic and molecular species drive plasma chemistry. Low-energy electrons, in particular, can access dissociative channels that lead to different chemical and electronic branching pathways. These, in turn, drive energy balance, neutral particle transport, and excited state dynamics. Such low-energy electron collisions take place in the low-temperature regions of fusion plasmas [1,2] and astrophysical environments [3]. N_2H^+ and its isotopolog N_2D^+ find specific utility as diagnostics of nitrogen and deuterium abundances in star forming regions and of dust chemistry in the interstellar medium [4,5]. Charge exchange and protonation reactions with species such as N_2H also play a key role in atmospheric environments [6]. This makes knowledge of destruction pathways essential in modeling plasma chemistry reaction chains and evolution.

The production of heavy-ion fragments from N_2D^+ due to electron scattering can proceed through various channels, as shown in Table I. The direct dissociative excitation process proceeds via a vertical transition to either a dissociative excited state or a bound excited state that couples to a dissociative pathway. Both of these pathways result in a charged ion fragment on dissociation. The resonant dissociative excitation process proceeds through the resonant capture of an electron to a neutral N_2D^* Rydberg state. This state then decays via autoionization and subsequent dissociation, producing a charged ion fragment and neutral fragments. We will refer to both of these processes jointly as dissociative excitation (DE).

The dissociative ionization (DI) process is similar to the DE process with the exception that an electron is removed from the system, resulting in at least two charged ion fragments. Given that two positively charged fragments are initially in close proximity at the time of dissociation, some amount of Coulomb force is experienced by the mutual repulsion of the charged fragments. This augments the kinetic energy release due to bond breaking in the dissociation process.

Two additional processes are not considered here; resonant ion-pair formation (RIP) and nondissociative ionization. While the RIP process can lead to heavy ion fragments, the cross sections for this process are typically small [7] and are not expected to contribute significantly to our investigation. Nondissociative ionization of the molecular cation species likewise has small cross sections and does not contribute to singly charged ion fragment measurements.

This paper is focused on low-energy electron scattering with N_2D^+. No previous experimental or theoretical work has focused on the electron-impact DE or DI of this molecular cation. However, there has been considerable interest in the dissociative recombination (DR) of this cation, particularly on the possible fragmentation dynamics of the N−N bond [8–10]. Despite early suggestions that DR could fracture the N−N bond efficiently, this is now believed to be a considerably less important fragmentation pathway.

The current study is a follow-up of the near-zero eV DR work with the aim of investigating dissociation dynamics of simple triatomic systems, relevant to plasma environments, at slightly higher electron collision energies of 5–100 eV, where DE and DI become the dominant dissociation processes. The measurements reported here are absolute cross sections for the production of N_2^+, ND^+, and N^+ fragments due to dissociation. At these higher electron energies, fracture of the N−N bond does become an important pathway.

II. EXPERIMENT

A. Ion beams

The molecular ion beam of $^{14}N_2D^+$ was produced in the Oak Ridge National Laboratory (ORNL) electron cyclotron resonance (ECR) ion source [11] using N_2 and D_2 working

*fogle@physics.auburn.edu

TABLE I. Processes for electron-impact dissociation of N_2D^+ ions producing N_2^+, ND^+, and N^+ fragment ions.

Process	Channel
Direct dissociative excitation	$e^- + N_2D^+ \rightarrow e^- + N_2^+ + D$
	$\rightarrow e^- + ND^+ + N$
	$\rightarrow e^- + N^+ + ND$
	$\rightarrow e^- + N^+ + N + D$
Resonant dissociative excitation	$e^- + N_2D^+ \rightarrow N_2D^* \rightarrow e^- + N_2^+ + D$
	$\rightarrow N_2D^* \rightarrow e^- + ND^+ + N$
	$\rightarrow N_2D^* \rightarrow e^- + N^+ + ND$
	$\rightarrow N_2D^* \rightarrow e^- + N^+ + N + D$
Dissociative ionization	$e^- + N_2D^+ \rightarrow 2e^- + N_2^+ + D^+$
	$\rightarrow 2e^- + ND^+ + N^+$
	$\rightarrow 2e^- + N^+ + N + D^+$
	$\rightarrow 2e^- + N^+ + N^+ + D$

gasses. The total working gas pressure in the ECR ion source was approximately 10^{-5} Torr and injected RF powers were a few watts at 10 GHz. The deuterated species was used solely for the purpose of separating the ion fragments produced during dissociation from the parent ion beam.

Ions produced by the ECR source were extracted to form a beam with an energy of 7 keV. The ion beam was subsequently momentum analyzed by a dipole magnet before being transported, via magnetic and electrostatic elements, to the crossed electron ion beams apparatus. Typical ion beam currents delivered to the crossed-beams apparatus range from 50 to 100 nA. Charge-to-mass contamination of the ion beam was checked by first operating the ECR ion source with D_2 working gas only and performing a mass scan with the dipole magnet after the source extraction. It was estimated that the analyzed N_2D^+ beam had no more than 3% impurities, which is considered negligible given the overall error estimation.

Given that the flight time from the ion source to the interaction region was on the order of a few microseconds, it is not expected that any vibrational excitations would relax before reaching the interaction region. Although the current experiment has no means to determine the initial rovibrational distribution of the parent molecular ions, it is expected that contributions to the cross section below the lowest threshold could be an indication of the excited state population. Ion source conditions were maintained with only minor adjustments during data acquisition so as to limit any variation in excited state populations.

B. Crossed-beams method

The ORNL crossed electron-ion beams apparatus is shown schematically in Fig. 1. Incident N_2D^+ molecular ions passed through a 90° electrostatic analyzer to remove any ions that may have undergone charge exchange or dissociative interactions with the residual gas of the vacuum system during beam transport. The analyzed molecular ion beam then passed through the interaction region perpendicular to

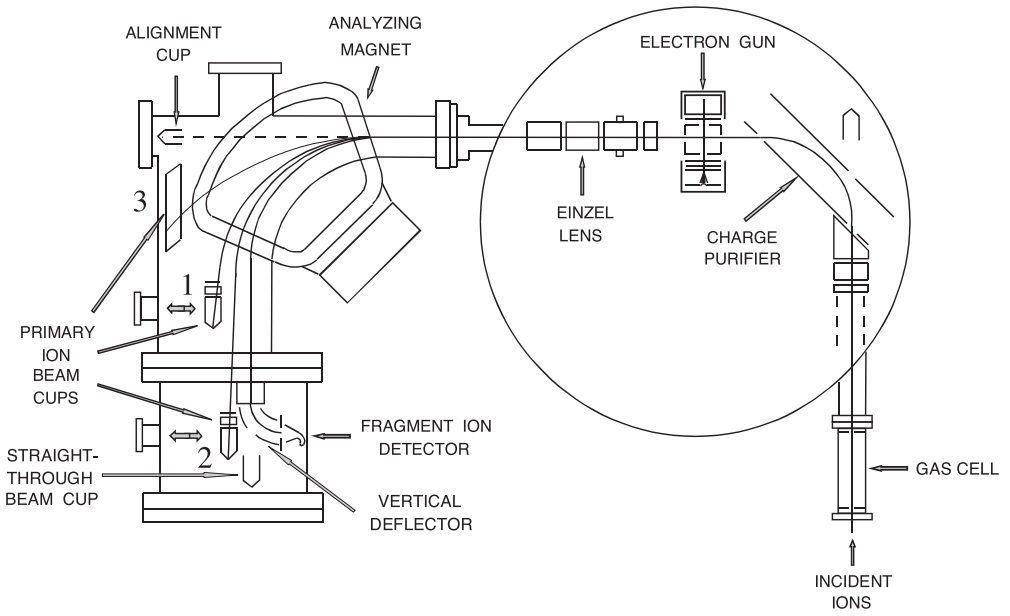

FIG. 1. ORNL crossed electron ion beams apparatus. See text for details.

the magnetically confined electron beam. The center-of-mass interaction energy was tuned by adjusting the extracted electron beam energy.

The details of the custom electron gun have been discussed previously [12,13]. Electrons are produced by an indirectly heated planar cathode and extracted over a uniform electrostatic field to define the electron beam energy. A 250-G magnetic field, coaxial to the electron gun direction, confines the electrons and, together with the extraction apertures, forms a uniform rectangular beam (approximately 2 mm wide and 10 mm in height) over the 2-mm interaction region. Opposite the interaction region, the electrons are collected by a Faraday cup constructed of stacked, tantalum, razor-edged blades oriented with the sharp edges toward the beam. The collector is biased by a +300 V battery to minimize electron loss that would lead to an inaccurate electron current measurement needed for absolute cross-section determinations. Typical electron beam currents are ∼10 μA at 10 eV and ∼250 μA at 100 eV. The electrons are chopped at 1 kHz in order to separate fragment ion signals due to electron impact as compared to collisions with the residual gas, which can be relatively large for the case of N_2^+ fragment ions where the rate of N_2D^+ deprotonation due to residual gas collisions is large.

Fragment ions produced by dissociation of the parent N_2D^+ ion beam leave the interaction region and are separated from the parent ion beam by a double-focusing dipole magnetic. Depending on the mass ratio of the fragment ion to the parent ion beam molecule, the parent beam is collected in one of three different Faraday cups used to measure the incident ion beam current. The fragment ions of interest are directed toward a vertical 90° electrostatic deflector which steer the fragment ions into a discrete dynode electron multiplier detector. The detector (ETP model 14880) has an acceptance window of 25 × 10 mm with the widest dimension oriented in the dispersion plane of the analyzing magnet to collect all of the ion fragments regardless of kinetic energy release during dissociation. This detector is capable of counting random particle impacts in excess of one million average events per second with little dead time. This capability was essential given that background signal rates for some of the ion fragment channels investigated were more than could be sustained by a conventional channel electron multiplier.

The dipole magnet following the interaction region was scanned to confirm complete collection of ion fragments and to verify that adjacent ion fragmentation channels, e.g., ND^+ and N^+, did not overlap spatially due to broad kinetic energy release distributions.

The absolute cross sections for N_2^+, ND^+, and N^+ fragment ion production were determined from measured quantities by

$$\sigma(E) = \frac{R}{I_i I_e} \frac{q e^2 v_i v_e}{\sqrt{v_i^2 + v_e^2}} \frac{F}{\epsilon}, \tag{1}$$

where $\sigma(E)$ is the absolute cross section at the center-of-mass energy E, R is the fragment ion signal rate, qe is the charge of the incident ions, v_i and v_e are the incident ion and electron velocities, ϵ is the detection efficiency (90%), and F is the form factor.

The overlap of the ion and electron beams in the direction orthogonal to both beams, here labeled the z direction, was measured at each interaction energy with a rotatable slit probe scanned across both the ion and electron beams in the interaction region. Current profiles of the ion and electron beams, $I_i(z)$ and $I_e(z)$, respectively, were measured independently and a form factor, F, was determined by

$$F = \frac{\int I_e(z)\,dz \int I_i(z)\,dz}{\int I_e(z) I_i(z)\,dz}. \tag{2}$$

TABLE II. Absolute experimental uncertainties. These uncertainties are combined with the relative uncertainties at a 90% confidence level to determine the total uncertainty in each data point.

Source of uncertainty	Uncertainty (%)
Product ion detection and pulse processing	±5
Transmission of product ion to detector	±4
Absolute value of form factor	±4
Ion current measurement	±2
Electron current measurement	±2
Ion velocity	±1
Electron velocity	±1
Quadrature sum	±8.2

The predominant systematic uncertainties associated with the experiment are listed in Table II with the estimated error for each component at a high confidence level (equivalent to a 90% confidence level for statistical uncertainties). These errors are treated as random sign errors, summed in quadrature, and combined with the statistical uncertainty of each data point (at a 90% confidence level) to determine the total uncertainty. Detailed discussions of the experimental uncertainties have been published previously by Bannister [14].

III. RESULTS AND DISCUSSION

The N_2D^+ cation has a linear ground-state geometry [15,16] best described by $C_{\infty v}$ symmetry. There are, however, bent excited states of C_s symmetry [16] which will not be covered here as the current experiment had no definitive means by which to determine that a geometry change was induced on electron impact. The ground-state configuration of N_2D^+ is $1\sigma^2\ 2\sigma^2\ 3\sigma^2\ 4\sigma^2\ 5\sigma^2\ 1\pi^4\ {}^1\Sigma^+$. Excitation of either the 5σ or 1π electrons correspond to the first several excited states. It has been pointed out by Gianturco and Materzanini [16] that the lowest-lying excited states of N_2H^+ are mainly made up of N_2^+ states while the first excited state of N_2 is much higher in energy.

Brites and Hochlaf [17] have made a theoretical study of the N_2H^{2+} dication, which is relevant to the DI channels observed in the current experiment. They suggest that the lowest-energy dication state, $^2\Sigma^+$, is one in which a 5σ electron is removed from the N_2H^+ ion. They show a dense set of dication excited state potential energy curves that also exhibit a number of avoided crossings arising from degenerate C_s symmetry geometries. These intersections allow for vibronic coupling between states and provide a path for fast predissociation mechanisms.

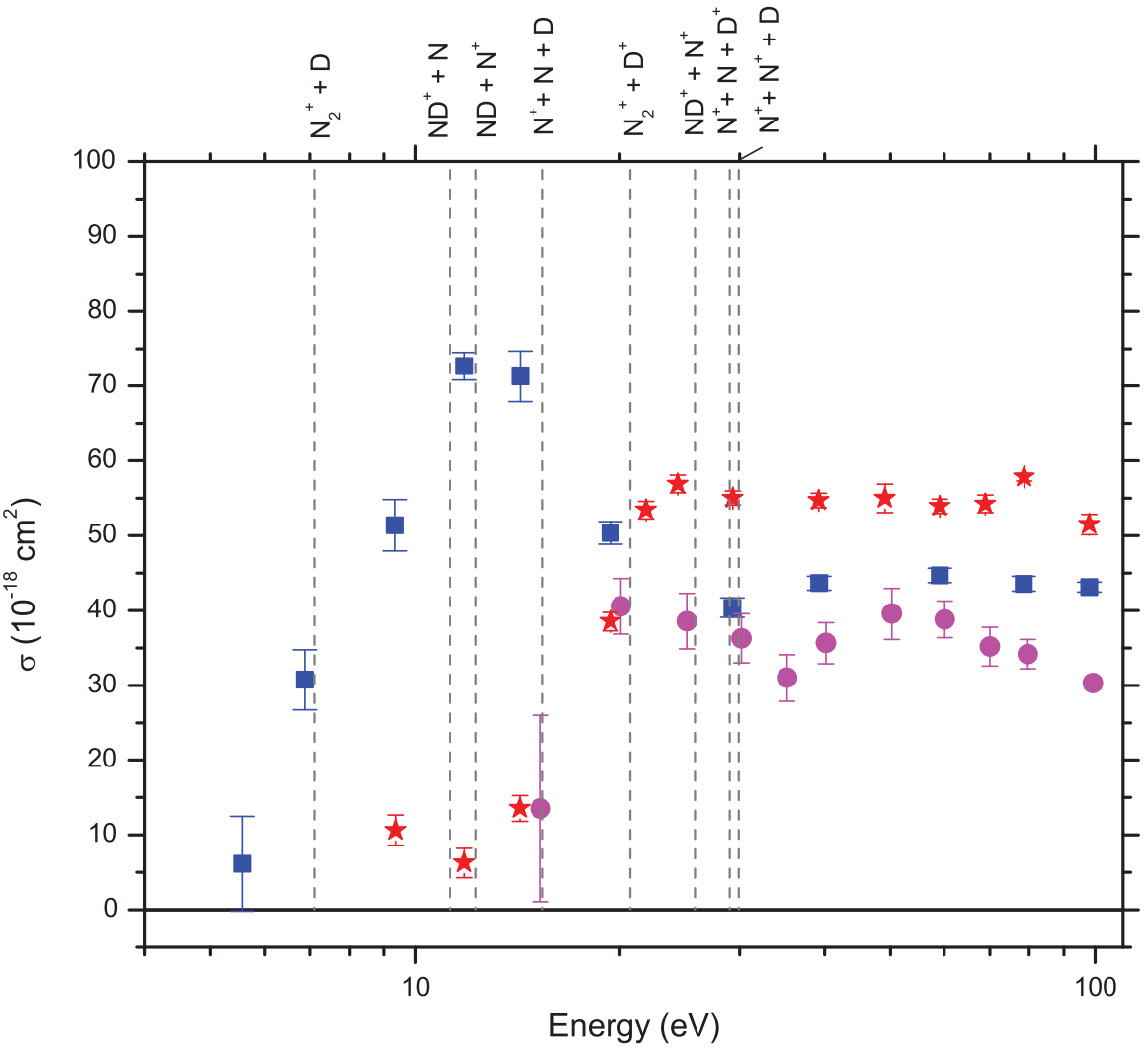

FIG. 2. (Color online) Absolute cross sections for DE and DI of N_2D^+ resulting in N_2^+ (squares), ND^+ (circles), and N^+ (stars) ion fragments. The thresholds for different dissociation channels are shown by the vertical dashed lines. See the text for more details regarding these thresholds.

Figure 2 shows the measured absolute DE and DI cross sections for N_2D^+ resulting in N_2^+, ND^+, and N^+ ion fragments. The tabular data are listed in Tables III–V. The thresholds for the various dissociation channels are also shown in Fig. 2. These dissociation channel thresholds are shown schematically in Fig. 3. The thresholds are determined by, first, establishing the neutral dissociation energies, i.e., corresponding to the kinetic energy release during dissociation due to DR producing ground-state fragments. It should be noted that the $N + N + D$ channel is energetically forbidden in DR but is shown in Fig. 3 since the energies relevant for DE and DI make the three-body dissociation channels accessible. The values for the neutral dissociation energies for the $N_2 + D$ and the $ND + N$ neutral dissociation channels are taken from Geppert *et al.* [8]. The DE and DI thresholds stemming from each of these channels is then determined by adding the corresponding ionization energies for N_2 (15.6 eV), ND (13.1 eV), N (14.5 eV), and D (13.6 eV). The energy for the three-body dissociation channel $N^+ + N + D^+$ is estimated by adding the proton affinity of N (3.6 eV) to the $ND^+ + N^+$ threshold. The other corresponding three-body channels are determined using the ionization energies mentioned previously. All of the ionization energies and proton affinity data are taken from the NIST Chemistry Webbook [18].

At low electron energies, only the DE process is available with four DE channels accessible in this energy range, $N_2^+ + D$, $ND^+ + N$, $ND + N^+$, and $N^+ + N + D$. As can be seen in Fig. 2, the $N_2^+ + D$ channel is the dominant heavy-ion fragment dissociation pathway on excitation. It is expected that the deprotonation cross section would be considerably larger but this channel could not be measured in the current experiment. There is also an underlying resonant-like structure centered at 12 eV for this channel. A similar structure was observed in the DE of BD_2^+ and CH_2^+ measured by Fogle *et al.* [19]. Clearly, a strongly coupled excitation channel exists within this energy region. The theoretical potential energy curves of Gianturco and Materzanini [16] indicate that the $2^1\Sigma^+$, $3^1\Sigma^+$, $4^1\Sigma^+$, and $1^1\Pi$ excited bound states lie 10–15 eV above the ground state. This is in reasonable agreement with the observed DE peak

TABLE III. Absolute cross sections for the formation of N^+ from N_2D^+.

E (eV)	$\sigma(E)$ (10^{-18} cm^2)
9.4	10.65 ± 2.0
11.8	6.27 ± 2.0
14.3	13.57 ± 1.7
19.4	38.53 ± 1.3
21.9	53.42 ± 1.2
24.4	56.90 ± 1.2
29.3	55.03 ± 0.9
39.2	54.72 ± 1.0
49.2	54.99 ± 1.9
59.1	53.92 ± 1.0
69.0	54.25 ± 1.2
78.7	57.83 ± 0.5
98.1	51.49 ± 1.4

of the current experiment and are likely the main contributing states (see Tables III–V).

For the $N_2^+ + D$ channel, there is also an indication of a positive cross section below the threshold. This is likely an indication of vibrational excitation in the initial parent cation. The ECR ion source is expected to produce vibrationally excited states and the few-microsecond transport time from the source to the interaction region is not expected to allow for any considerable de-excitation of these states.

The other DE channels, $ND^+ + N$, $ND + N^+$, and $N^+ + N + D$, lead to N−N bond breaking where N^+ and ND^+ ion fragments are formed. The experimental cross sections for producing these fragments seem to rise at comparable rates as a function of electron energy with a marked divergence around 20 eV.

At electron energies above ∼20 eV, the DI thresholds are reached and multiple ion fragments can be produced. There are two distinct two-body DI channels, $N_2^+ + D^+$ and $ND^+ + N^+$. As can been seen in Fig. 2, the cross sections for these channels are comparable. It should be noted that the $ND^+ + N^+$ channel is measured twice in this experiment, once by measuring ND^+ fragment production and again by measuring N^+ fragment production. The DI cross section should be the same regardless of the fragment ion measured; however, the experiment measures

TABLE IV. Absolute cross sections for the formation of N_2^+ from N_2D^+.

E (eV)	$\sigma(E)$ (10^{-18} cm^2)
5.6	6.15 ± 6.4
6.9	30.74 ± 4.0
9.3	51.40 ± 3.4
11.8	72.66 ± 1.8
14.3	71.29 ± 3.3
19.4	50.37 ± 1.5
29.3	40.38 ± 1.3
39.3	43.65 ± 0.9
59.1	44.68 ± 1.0
78.6	43.57 ± 1.0
98.0	43.12 ± 0.7

TABLE V. Absolute cross sections for the formation of ND^+ from N_2D^+.

E (eV)	$\sigma(E)$ (10^{-18} cm^2)
15.3	13.53 ± 12.5
20.1	40.56 ± 3.7
25.1	38.56 ± 3.7
30.2	36.28 ± 3.3
35.3	31.00 ± 3.1
40.2	35.63 ± 2.7
50.2	39.54 ± 3.4
60.1	38.81 ± 2.4
70.0	35.16 ± 2.6
79.7	34.15 ± 2.0
99.3	30.30 ± 0.8

total cross sections and thus any difference in the underlying DE leading to ND^+ and N^+ fragment production would be included in the DI region. The observed difference in the ND^+ and N^+ fragment measurements in the DI region could also be attributed to three-body break up into the $N^+ + N + D$, $N^+ + N^+ + D$, and $N^+ + N + D^+$ channels noted in Fig. 3. The $N^+ + N + D$ DE channel has a threshold below the observed divergence of the ND^+ and N^+ fragment cross sections and could be a contributor to the observed enhancement to N^+ production. However, the observed divergence is below the three-body DI thresholds, making it less likely that these channels contribute.

Similar measurements of DE and DI of C_2D^+ have been made by Lecointre *et al.* [20]. It is interesting to note

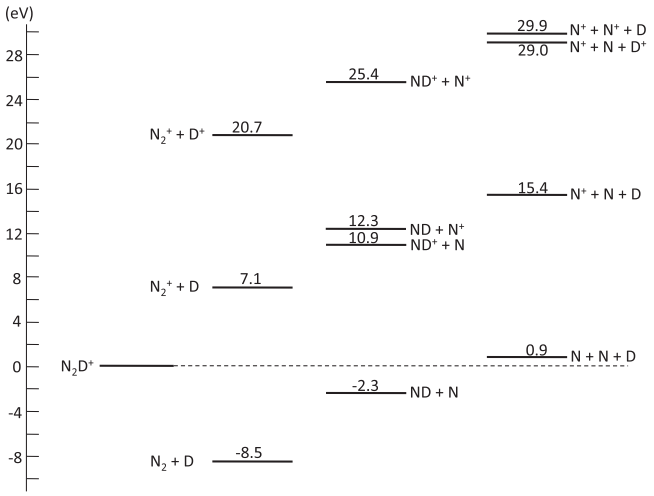

FIG. 3. Energy diagram of DE and DI thresholds of N_2D^+ have been determined from the neutral dissociation energies for different dissociation channels (see text for more detail). The different DE and DI channels are determined by adding the respective ionization potentials of N_2, ND, N, and D to these base neutral dissociation energies. The thresholds for the three-body channels are derived by adding the proton affinity of N to the $ND^+ + N^+$ channel to determine the $N^+ + N + D^+$ threshold and, likewise, using ionization energies to determine the other three-body channel thresholds.

that they observe similar cross-section features for C_2^+ and CD^+ ion fragment formation and that they observe the C^+ production to be dominant over C_2^+, while, for N_2D^+, we observe a completely different dynamic, with N_2^+ being the dominant channel. Their results are not surprising in light of DR measures for C_2D^+ that showed a propensity to three-body fragmentation [21]. For N_2D^+, however, the three-body dissociation channel is energetically inaccessible in DR and only two-body fragmentation occurs. This is mirrored in the current results for DE and DI.

IV. CONCLUSION

The absolute cross sections for the production of N_2^+, ND^+, and N^+ ion fragments due to electron-impact dissociative excitation and ionization of N_2D^+ have been measured using the crossed beams apparatus at Oak Ridge National Laboratory over the energy range of 5–100 eV. It is observed that the $N_2^+ + D$ channel is the predominant DE pathway below 20 eV and is likely due to excitation to the $2^1\Sigma^+$, $3^1\Sigma^+$, $4^1\Sigma^+$, and $1^1\Pi$ excited bound states predicted theoretically by Gianturco and Materzanini [16]. This channel also exhibits a strong resonant-like structure centered at 12 eV, similar to structures observed in previous measurements for dihydride cations [19]. In the DI regime above 20 eV, N−N bond breaking becomes more prevalent with the $ND^+ + N^+$, $N_2^+ + D^+$, and, possibly, the $N^+ + N + D$ channels being the main contributors. There is a marked divergence in the DE cross section for the ND^+ and N^+ ion fragments at ∼20 eV. This divergence occurs below the three-body DI thresholds, making them less likely a contributing factor; however, the $N^+ + N + D$ threshold is below the observed divergence and could indicate a possible three-body contribution to N^+ production.

ACKNOWLEDGMENTS

This research was supported in part by the Office of Fusion Energy Sciences and the Division of Chemical Sciences, Geosciences, and Biosciences, Office of Basic Energy Sciences of the US Department of Energy. One of the authors (S.D.) gratefully acknowledges support from the ORNL Postdoctoral Research Associates Program administered jointly by the Oak Ridge Institute for Science and Education and Oak Ridge National Laboratory.

[1] H. Tawara, in *Atomic and Molecular Processes in Fusion Plasmas*, edited by R. K. Janev (Plenum, New York, 1995), pp. 461–496.
[2] R. K. Janev and D. Reiter, Phys. Plasmas **9**, 4071 (2002).
[3] A. Dalgarno, in *Atomic Processes and Applications*, edited by P. G. Burke and B. L. Moiseiwitsch (North-Holland, Amsterdam, 1976), pp. 109–132.
[4] P. Thaddeus and B. Turner, Astrophys. J. **201**, L25 (1975).
[5] L. Snyder, J. Hollis, D. Buhl, and W. Watson, Astrophys. J. **218**, L61 (1977).
[6] V. Brites and M. Hochlaf, J. Phys. Chem. A **113**, 11107 (2009).
[7] W. Zong, G. Dunn, N. Djuric, M. Larsson, C. Greene, A. AL-Khalili, A. Neau, A. Derkatch, L. Vikor, W. Shi *et al.*, Phys. Rev. Lett. **83**, 951 (1999).
[8] W. D. Geppert, R. Thomas, J. Semaniak, A. Ehlerding, T. J. Miller, F. Osterdahl, M. af Ugglas, N. Djuric, A. Paal, and M. Larsson, Astrophys. J. **609**, 459 (2004).
[9] D. Talbi, Chem. Phys. **332**, 298 (2007).
[10] N. Adams, C. Molek, and J. McLain, J. Phys.: Conf. Ser. **192**, 012004 (2009).
[11] F. W. Meyer, in *Trapping Highly Charged Ions: Fundamentals and Applications*, edited by J. Gillaspy (Nova Science, Huntington, NY, 2001), p. 117.
[12] P. O. Taylor, K. T. Dolder, W. E. Kauppila, and G. H. Dunn, Rev. Sci. Instrum. **45**, 538 (1974).
[13] D. C. Gregory, F. W. Meyer, A. Müller, and P. Defrance, Phys. Rev. A **34**, 3657 (1986).
[14] M. E. Bannister, Phys. Rev. A **54**, 1435 (1996).
[15] K. Vasudevan, S. Peyerimhoff, and R. Buenker, Chem. Phys. **5**, 149 (1974).
[16] F. Gianturco and G. Materzanini, Eur. Phys. J. D **4**, 321 (1998).
[17] V. Brites and M. Hochlaf, Chem. Phys. Lett. **477**, 48 (2009).
[18] *NIST Chemistry WebBook, NIST Standard Reference Database Number 69* (2011), [http://webbook.nist.gov/chemistry/].
[19] M. Fogle, E. M. Bahati, M. E. Bannister, S. H. M. Deng, C. R. Vane, R. D. Thomas, and V. Zhaunerchyk, Phys. Rev. A **82**, 042720 (2010).
[20] J. Lecointre, H. Cherkani-Hassani, S. Cherkani-Hassani, D. Belic, J. Jureta, and P. Defrance, Eur. Phys. J. D **60**, 331 (2010).
[21] A. Ehlerding, F. Hellberg, R. Thomas, S. Kalhori, A. Viggiano, S. Arnold, M. Larsson, and M. af Ugglas, Phys. Chem. Chem. Phys. **6**, 949 (2004).